**Rational Design of Original Fused-cycle Selective Inhibitors of Tryptophan 2,3-Dioxygenase**

Arina Kozlova[1,2,3], Léopold Thabault[1,4], Maxime Liberelle[1], Simon Klaessens[2,3], Julien R.C. Prévost[1], Caroline Mathieu[1], Luc Pilotte[2,3], Vincent Stroobant[2,3], Benoît Van den Eynde[2,3,5], Raphaël Frédérick[1*].

[1] Louvain Drug Research Institute (LDRI), Université catholique de Louvain (UCLouvain), B-1200 Brussels, Belgium.

[2]Ludwig Institute for Cancer Research, Brussels B-1200, Belgium.

[3] de Duve Institute, UCLouvain, Brussels B-1200, Belgium.

[4] Pole of Pharmacology and Therapeutics, Institut de Recherche Expérimentale et Clinique (IREC), UCLouvain,B-1200 Brussels, Belgium.

[5] Walloon Excellence in Life Sciences and Biotechnology, Brussels B-1200, Belgium.

* Correspondence and Lead Contact: Raphaël Frédérick

Mailing address: LDRI, Avenue Mounier 73/B1.73.10, B-1200 Brussels, Belgium.

Phone number: +32 2 764 73 41

Email address: raphael.frederick@uclouvain.be

**ABSTRACT**

Tryptophan-2,3-dioxygenase (TDO2) is a heme-containing dioxygenase constitutively expressed at high concentrations in the liver and responsible for L-Tryptophan (L-Trp) homeostasis. Expression of TDO2 in cancer cells results in the inhibition of the immune-mediated tumor rejection due to an enhancement of the L-Trp catabolism via the kynurenine pathway. In the study herein, we disclose a new 6-(1H-indol-3-yl)-benzotriazole scaffold of TDO2 inhibitors developed through rational design, starting from existing inhibitors. Modulations of the initial scaffold led to the synthesis of highly stable compounds displaying a nanomolar potency and a better understanding of the structural modulations that could be accommodated inside the active site of *h*TDO2.

**Graphical abstract:**

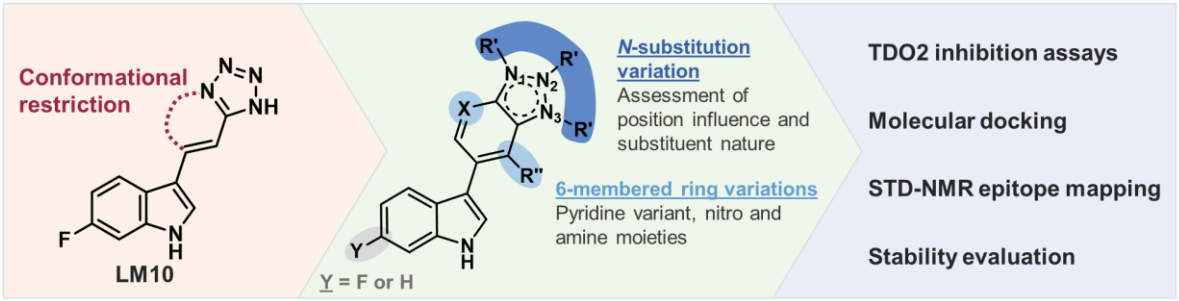


- **INTRODUCTION**

Multiple immune resistance mechanisms are often involved within a tumor microenvironment, hampering the immune response and leading to the failure of currently available treatments.[1,2] As we progress towards an individualized treatment approach, there is a need for new tools to overcome these hurdles. Using small-molecule inhibitors (SMIs) to target tolerogenic pathways is an attractive strategy for cancer immunotherapy. The advantages of SMIs reside in their ability to reach a wide array of intracellular targets, the possibility to fine-tune their ADME properties, as well as their superior cost-effectiveness compared to biologics.[3,4] Within this context, small-molecular scaffolds are a rapidly expanding area of research, as exemplified by the increasing number of patent applications and compounds currently under evaluation at preclinical and clinical stages both as stand-alone or combination therapies.[3–5]

Enzymes of the tryptophan-kynurenine pathway (KP), such as indoleamine-2,3-dioxygenase 1 (IDO1), tryptophan-2,3-dioxygenase (TDO2) or kynurenine-3-monooxygenase (KMO), are attractive drug targets for cancer immunotherapy.[6,7] Catabolism of L-Trp promotes an immunosuppressive environment both through the depletion of this essential amino acid and the accumulation of kynurenine (KYN) metabolites.[8] Firstly, a decrease in L-Trp levels results in a blockage of CD8+ and CD4+ T-cells, in the G1 cell cycle phase, due to their susceptibility to the amino acid shortage.[9] Secondly, it leads to the activation of the GCN2 "stress" sensing kinase, further hindering CD8+ T-cell proliferation.[10] Finally, immunosuppression from L-Trp deprivation might also be linked to the inhibition of the mammalian target of the rapamycin (mTOR) pathway.[11]

On the other hand, along with its catabolites, kynurenine (KYN) favors regulatory T cells (Tregs) through several mechanisms. One of the currently proposed mechanism resides in the interaction between KYN and the aryl hydrocarbon receptor (AHR), leading to the polarization of CD4+ T-cells into the $T_{reg}$ phenotype.[12–14]

Overall, excessive KP activation promotes carcinogenesis and tumor cell growth by reducing T-cell proliferation, suppressing natural killer cells (NK), promoting Treg differentiation, and activating, recruiting, and expanding myeloid-derived suppressor cells (MDSCs).[15,16]

This implication of the KP in tumor immune escape has led to considerable efforts from the medicinal chemist community to develop SMI to interfere with this pathway. Most notably, the development of SMI for IDO1 has received tremendous attention since the discovery of its implications in cancer immune escape.[17,18] Although the outcomes of IDO1 inhibitors in clinical trials did not meet expectations for several possible reasons discussed in a recently published review, the KP remains a reservoir of attractive targets and an active research area.[19,20]

Much like IDO1, TDO2 independently catalyzes the first and rate-limiting step of the KP: the oxidative cleavage of L-Trp pyrrole moiety to form *N*-formylkynurenine. TDO2 plays a central role in the regulation of systemic L-Trp concentration.[21] Despite sharing the same enzymatic reaction, TDO2 only shares around 10 % sequence identity with IDO1 and is much more specific for L-Trp.[22,23] Numerous human tumors, including glioblastoma, melanoma and liver, bladder, pancreatic and colon carcinomas, express TDO2 at various levels to exploit the KP as an immune escape mechanism.[24,25] TDO2 inhibitors would be particularly relevant in hepatocarcinoma, 100 % of which express this enzyme.[24,26]

This interest in TDO2 inhibition led to the development of several families of TDO2 inhibitors, as exemplified by some patents and few articles published to date.[27–30] We previously established initial structure-activity relationships (SARs) for a series of TDO2-selective and competitive inhibitors characterized by a 3-(2-(pyridyl)ethenyl)indole scaffold that demonstrated several prerequisites for TDO2 inhibition and potential for optimization.[31] A thorough exploration of SARs around the initial

**680C91** inhibitor (**Table 1**) drew the first prerequisite for TDO2 inhibition by catalytic-site inhibitors. To summarize, all investigated replacements of indole moiety led to inactive compounds, even when changes were minor (5-azaindole or indazole). Moreover, the indole nitrogen should remain free, and only substitution in C5 or C6 with small lipophilic substituents such as fluorine led to increased potency. As suggested by molecular docking, the 3-pyridyl group of **680C91** is found in the vicinity of Arg-144 guanidinium. Accordingly, the replacement of this 3-pyridyl with H-bond acceptors or negatively charged groups provided more soluble compounds that could be further stabilized in the TDO2 binding cleft through ionic interactions.[31] Replacement of the trans-vinyl linker to longer, shorter, or a more flexible ethyl spacer resulted in inactive or poorly active derivatives. Thus, it appeared that TDO2 was particularly susceptible to small modifications of the inhibitor. Recent crystallographic studies revealed that the active site of *h*TDO2 was, in fact, more rigid than that of *h*IDO1, which has a broader substrate specificity.[32]

Hence, our previous research eventually led to the identification of **LM10** (**Figure 1**), characterized by a *trans*-vinyl tetrazole side chain in the 3-position of a 6-fluoroindole scaffold and a low micromolar ($\mu$M) potency. The administration of **LM10** restored the immune response and promoted tumor rejection in a mouse model.[24] **LM10** was, to our knowledge, the very first soluble and bioavailable TDO2 inhibitor demonstrating preclinical anti-tumor efficacy and thus the proof-of-concept of TDO2 inhibition for anticancer immunotherapy.[24] Lately, inhibition of TDO2 was also demonstrated to be beneficial for the efficacy of immune checkpoint inhibitors like anti-PD1 and anti-CTLA4 monoclonal antibodies.[25] Interestingly, the benefit of TDO2 blockade persisted even in the absence of its tumoral expression, probably due to the increased availability of circulating L-Trp levels.[25]

Our previous work provided useful data for TDO2 inhibitors development, exemplified by numerous publications and patents reporting TDO2 inhibitors based on the 6-*F*-indole pharmacophore.[27] However, the LM10 series suffered from several drawbacks, which prevented its further therapeutic application. First, the TDO2 inhibitory potency in this series could not be much improved and could not

reach a cellular efficacy below the $\mu$M threshold. Furthermore, we could not find a replacement for the electrophilic vinyl linker prone to chemical instability (trans-cis isomerization), side reactions (Michael acceptor), and metabolic liabilities. In the present work, to further expand SARs data for TDO2 and provide a better molecular framework for TDO2 inhibitors, we designed, synthesized, and evaluated a series of original, highly stable, and selective TDO2 inhibitors.

## ■ RESULTS AND DISCUSSION

**Design of TDO2 Inhibitors.** We first reasoned that the rigidification of the lateral *trans*-vinyl in the **680C91** and **LM10** scaffolds could improve the TDO2 inhibitory potency by conformational restriction and provide a molecular template devoid of chemical liabilities (**Figure 1**). Moreover, several fused-cycle scaffolds were previously reported in a patent regarding TDO2 inhibitors, suggesting that such rigidification could lead to potent TDO2 inhibitors.[33] To investigate the impact of this replacement, we synthesized several fused-cycle analogues of **680C91** and **LM10** (**1 - 6**, **Table 1**). As indicated by our previous results, fluorine substitution in the 6-position of the indole usually leads to a slight increase in TDO2 inhibitory potency.[31] However, we first decided to avoid 6-fluorine derivatives as their synthesis results, in our experience, to lower yields compared to their non-fluorinated counterparts. Evaluation of these compounds in enzyme and cell-based assays on IDO1 and TDO2 demonstrated their ability to selectively inhibit TDO2. Interestingly, inhibition data on isolated enzyme assay is often lacking for reported TDO2 inhibitors. Indeed, several reported series of TDO2 inhibitors were characterized only by cell-based inhibition assays, which limits the SARs understanding and hence the future development of inhibitors.[27,28] We used the most commonly described assay for IDO1/TDO2 activity which follows the formation of the enzymatic product *N*'-formylkynurenine after hydrolysis with trichloroacetic acid and reaction with *p*-dimethylaminobenzaldehyde.[34,35] Regarding cell-based evaluation, we used a previously described assay using *h*TDO2-expressing P815B murine mastocytoma cell line.[24]

Compounds **1** to **6** all exhibited low $\mu$M range enzymatic $IC_{50}$s and mid-nanomolar (nM) to low $\mu$M activities in cells. Interestingly, these compounds also presented very low cellular toxicity, as assessed by our MTS assay (**Table 1**).

To rank and compare these initial hits, we normalized their respective affinities using ligand efficiency (LE: $1.4(-\log IC_{50})/(\text{heavy atom count})$) and lipophilic ligand efficiency (LLE: $pIC_{50} - \text{clog}D_{7.4}$) metrics.[36,37] These values allow us to consider both activity and lipophilicity,[2] an equally important attribute in drug design affecting ligand association and ADME properties.[38]

Isoquinoline analogues **1** and **2** were the most active compounds in cells, whereas quinazolines (**3**, **4**) showed a loss in their potency and LE/LLE values. Despite being less potent in cells than **1** and **2**, hit compound **6**, bearing a triazole moiety, had the lowest $IC_{50}$(enz) on *h*TDO2 and overall more favorable metrics due to its higher hydrophilicity and heteroatoms count. In addition to the absence of cell toxicity even at high concentrations (> 100 $\mu$M), incubation of cells with **6** did not affect the cell cycle distribution, which was determined by flow cytometry with propidium iodide DNA staining (PI) (**Figure S1**).

Evaluation of *h*TDO2 inhibition by **6** demonstrated an $IC_{50}(CI_{95\%})$ of 2.7 $\mu$M in the enzymatic assay ($IC_{50}$(enz)) and 0.8 $\mu$M in cell-based settings ($IC_{50}$(cell)), while **LM10** had an $IC_{50}$(enz) of 7.3 $\mu$M and an $IC_{50}$(cell) of 2.8 $\mu$M. Consequently, we decided to use **6** as a starting point for designing variously *N*-substituted original indole 3-benzotriazoles. However, compound **6** displayed worsened parameters (LLE = 2.56, $\text{cLog}D_{7.4}$=3.01) compared to **LM10** (LLE=4.99, $\text{cLog}D_{7.4}$=0.15), due to the loss of the tetrazole function, ionized at the physiological pH of 7.4. Thus, our optimization included benzotriazole substitutions of various hydrophobicity ranges aimed at probing TDO2 inhibition while considering their potency and physicochemical characteristics. Then, we further modulated the benzotriazole ring by (i) replacement with a triazolo-pyridine scaffold and (ii) substitution on the 6-membered ring of the benzotriazole.

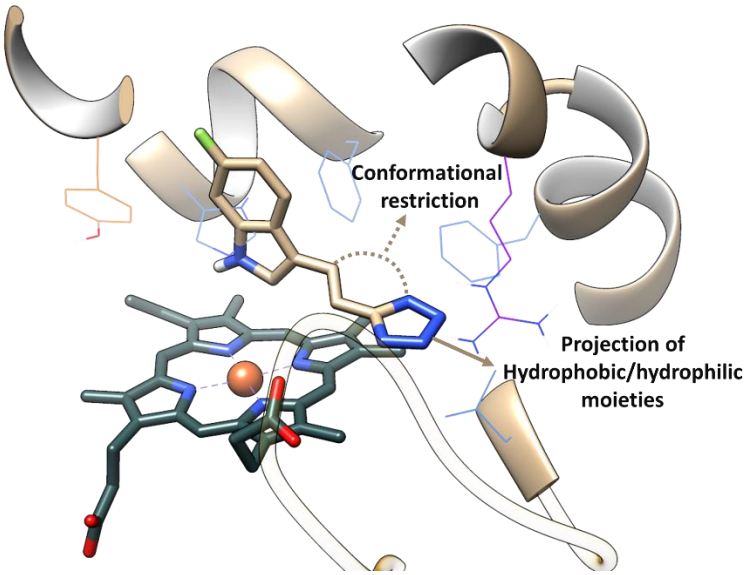


**Figure 1.** Molecular modelling of **LM10** inside *h*TDO2 active site (PDB code 5TI9)[39] and optimization strategy considered in this work.

**Table 1. 680C91**, **LM10** and their fused-cycle analogues (**1** – **6**) with their inhibition data.

| | 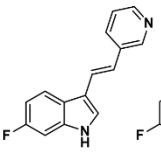 680C91 | 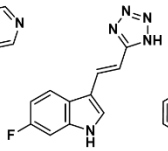 LM10 | 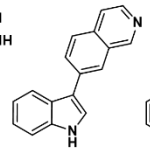 1 | 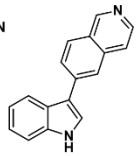 2 | 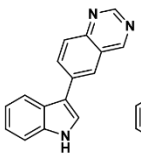 3 | 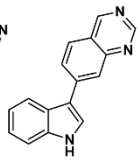 4 | 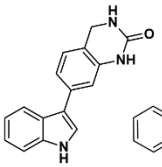 5 | 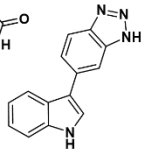 6 |
|---|---|---|---|---|---|---|---|---|
| *h*TDO2 **$IC_{50}$(enz)**[a] ($\mu$M) **$IC_{50}$(cell)**[a] | Ki 0.88[d]<br>0.28[d] | [6.1 – 8.7]<br>[1.74 – 6.62] | [5.6 – 7.1]<br>[0.07 – 0.12] | [4.9 – 6.6]<br>[0.10 – 0.14] | [12.8 – 16.9]<br>[0.27 – 0.40] | [21.2 – 32.6]<br>[0.49 – 0.66] | [12.7 – 22.9]<br>[0.83 – 1.16] | [2.0 – 3.4]<br>[0.70 – 1.02] |
| *h*IDO1 **$IC_{50}$(enz)** **$IC_{50}$(cell)** | *NI*[e] | *NI* | *NI* | *NI* | *NI* | *NI* | *NI* | *NI* |
| **LD50**[b] ($\mu$M) | > 80[d] | > 100 | > 20 | > 30 | > 100 | > 100 | > 30 | > 100 |
| **$cLogD_{7.4}$**[c] | 3.34 | 0.15 | 3.49 | 3.49 | 3.17 | 3.17 | 2.60 | 3.01 |
| **LLE** | 2.72 | 4.99 | 1.76 | 1.75 | 1.67 | 1.46 | 2.18 | 2.56 |
| **LE** | 0.46 | 0.41 | 0.38 | 0.38 | 0.35 | 0.33 | 0.33 | 0.42 |

[a] 95 % confidence intervals. Reported $IC_{50}$ values are calculated from measurements performed in triplicates, in at least two separate experiments. [b] Toxicity was determined using an MTS assay on P815B cell. [c] $LogD_{7.4}$ were calculated using Chemicalize. [d] Previously obtained data from *Pilotte et al.*[24] [e] *NI*: No inhibition at 100 $\mu$M.

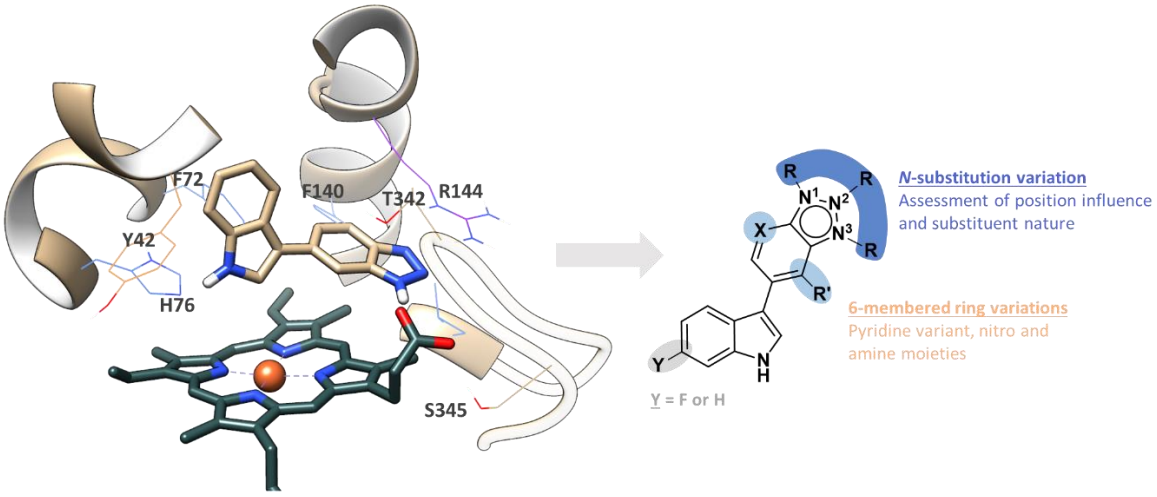


**Figure 2.** Molecular modelling of **6** inside hTDO2 active site (PDB code 5TI9)[39] and envisioned modulations around this scaffold.

**Structure-Activity Relationships of Benzotriazole Analogues.** We next synthesized a chemical library of benzotriazole analogues and evaluated the synthesized compounds for their ability to inhibit TDO2 both *in vitro*, using a purified truncated form of TDO2, and *in cellulo* using TDO2-expressing P815B cells.[23] To remain under initial velocity conditions, the assay was optimized so that cells consume less than 25 % of the available L-Trp. The same evaluation was performed on IDO1 to assess the selectivity towards TDO2 and demonstrated that none of these compounds could inhibit IDO1 (data not shown).

The active site of TDO2 is highly hydrophobic and relatively small, suggesting that an increase in potency could be achieved by adding lipophilic substituents to the initial scaffold of **6** ($IC_{50}$(enz): 2.7 $\mu$M/ $IC_{50}$(cell): 0.8 $\mu$M). To that end, we examined if the *N*-alkylation of the benzotriazole moiety would result in more potent compounds. Interestingly, The *N*-methyl analogues (**7**, **8**, **9**) displayed a significant gain in $IC_{50}$(cell) (up to 5-fold for ***7***) compared to their parent compound **6**, while maintaining a similar $IC_{50}$(enz) (**Table 2**). These results can be explained by the increase in the $LogD_{7.4}$ value resulting from the *N*-methylation. For SARs purposes, we next took an interest in further modifying the *N*-methyl analogues (**7**, **8**, **9**). We thus synthesized and evaluated compounds **10** to **16**, modified on the 6-membered ring of the benzotriazole. Our docking studies suggested that molecules **10**, **11**, **12** could form an H-bond with heme propionate through their aniline. The most potent

molecule remained the $N_2$ analogue **10**. The affinity of these compounds was not significantly different from their precursors, but their lower $cLogD_{7.4}$ value resulted in a better LLE (**Table 2**). Of note, the replacement of the benzotriazole by a 4-*aza*-benzotriazole in compounds **13**, **14** and **15**, did not result in better activities.

Next, we investigated the impact of bulkier *N*-chain substituents in $N_1$ and $N_3$ positions of the benzotriazole (compounds **17** to **40**). As the $N_2$ substitution was poorly available to alkylation, which only occurred through direct methylation of the benzotriazole, we investigated only $N_1$ and $N_3$ substitutions. Lipophilic substituents such as trifluoroethyl (**17**, **18**) and ethyl-cyclopropyl (**19**, **20**) yielded potent compounds, as expected from their higher $cLogD_{7.4}$. We quickly noticed that $N_1$-substitution was generally more favorable than $N_3$ for the activity. Interestingly, this trend was not apparent for the smaller methyl group as compounds **7**, **8** and **9** exhibit the same activity. For example, $N_1$-substitution with a trifluoroethyl (**18**, $IC_{50}$(enz):1.9 $\mu$M/ $IC_{50}$(cell)$_I$: 0.19 $\mu$M) resulted in a 3 to 7-fold increase in activity compared to $N_3$ substitution of the same moiety (**17**, $IC_{50}$(enz): 15.0 $\mu$M/ $IC_{50}$(cell): 0.44 $\mu$M). However, *N*-substitution by the less lipophilic acetamide moiety (**21**, **22**) resulted in less potent TDO2 inhibitors with similar affinity, although the $N_1$ substituted compound **22** appeared 2-fold more potent in cells than its isomer. Surprisingly, their hydrolyzed counterparts **23** and **24** displayed a loss of activity in both cellular and biochemical assays, suggesting that a low membrane permeability was not the only reason that could account for their poor activity. Compounds **25** and **26**, displaying a 2-(dimethylamino)ethyl moiety, shared a similar potency, perhaps due to the more flexible nature of their *N*-substituent. A further increase of *N*-substituent size with physiologically no*n*-ionized moieties (**27** to **32**) led to a systematic loss of activity and an increasing gap between cellular and enzymatic potencies. Interestingly, the introduction of longer *N*-substituents with H-bond donors such as piperidine (**33**, **34**) and pyrrolidine (**35**, **36**) led to a better activity for $N_3$-substituted compounds. Of note, these compounds had the best LLE values of all studied compounds due to their predominantly protonated state at physiological pH, resulting in low $cLogD_{7.4}$ values.

We also investigated a substitution of the indole ring $H_6$ to fluorine, with the synthesis of compounds **8a** and **37a**. As expected from previous results,[40] substitution with fluorine in this position of the indole was beneficial for the activity, and compound **37a** demonstrated a 5-fold increase in activity in both cellular and enzymatic assays ($IC_{50}$(enz): 5.2 $\mu$M/ $IC_{50}$(cell): 0.23 $\mu$M) compared to **37** ($IC_{50}$(enz): 24.9 $\mu$M/ $IC_{50}$(cell): 0.74 $\mu$M). The same gain in activity occurred for **8a** in cells ($IC_{50}$(enz): 1.1 $\mu$M , $IC_{50}$(cell): 0.02 $\mu$M) compared to **8**.

**Table 2. Inhibitory affinities ($IC_{50}$) of compounds against hTDO2 in the spectrophotometric assay and P815B cells.**

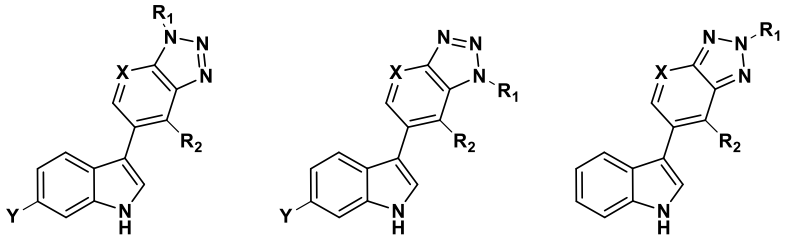


$N_3$ $N_1$ $N_2$

| N° | $N_x$ | Y | X | $R_2$ | $R_1$ | $IC_{50}$[a] ($\mu$M) Enz. | $IC_{50}$[a] ($\mu$M) Cell | Log$D_{7.4}$ [b] | LLE | LE |
|---|---|---|---|---|---|---|---|---|---|---|
| **7** | $N_2$ | | | | | 4.0 | 0.17 | 3.23 | 2.17 | 0.39 |
| **8** | $N_3$ | | | | | 3.87 | 0.22 | 3.17 | 2.24 | 0.39 |
| **9** | $N_1$ | | | | | 6.02 | 0.38 | 3.17 | 2.05 | 0.38 |
| **10** | $N_2$ | | | $NH_2$ | | 3.85 | 0.42 | 2.34 | 3.07 | 0.37 |
| **11** | $N_3$ | | | $NH_2$ | | 5.01 | 0.98 | 2.34 | 2.96 | 0.36 |
| **12** | $N_1$ | | | $NH_2$ | *$CH_3$ | 3.93 | 0.97 | 2.34 | 3.07 | 0.37 |
| **13** | $N_2$ | | N | | | 13.06 | 0.48 | 2.73 | 2.15 | 0.33 |
| **14** | $N_3$ | | N | | | 7.83 | 0.40 | 2.71 | 2.40 | 0.35 |
| **15** | $N_1$ | | N | | | 9.08 | 0.71 | 2.66 | 2.38 | 0.35 |
| **16** | $N_1$ | | | $NO_2$ | | 1.32[c] | 0.54 | 2.52 | 3.36 | 0.37 |
| **8a** | $N_3$ | F | | | | 1.1 | 0.02 | 3.31 | 2.65 | 0.41 |
| **17** | $N_3$ | | | | *$CF_3$ | 15.0 | 0.44 | 4.13 | 0.69 | 0.29 |
| **18** | $N_1$ | | | | | 1.9 | 0.19 | | 1.59 | 0.34 |
| **19** | $N_3$ | | | | * | 13.5 | 0.98 | 3.95 | 0.92 | 0.30 |
| **20** | $N_1$ | | | | | 3.9 | 0.10 | | 1.46 | 0.34 |
| **21** | $N_3$ | | | | *$CONH_2$ | 39.7 | 1.62 | 1.84 | 2.56 | 0.28 |
| **22** | $N_1$ | | | | | 36.1 | 0.68 | | 2.60 | 0.28 |
| **23** | $N_3$ | | | | *COOH | 173.8 | NI[d] | - 1.00 | 4.76 | 0.22 |
| **24** | $N_1$ | | | | | 104.5 | NI | | 4.98 | 0.25 |
| **25** | $N_3$ | | | | * N | 36.9 | 1.93 | 1.70 | 2.73 | 0.26 |
| **26** | $N_1$ | | | | | 24.6 | 1.64 | | 2.91 | 0.27 |
| **27** | $N_3$ | | | | * O | 44.1 | 1.86 | 3.19 | 1.16 | 0.25 |
| **28** | $N_1$ | | | | | 21.9 | 0.41 | | 1.44 | 0.26 |

| | | | | | | | | | |
|---|---|---|---|---|---|---|---|---|---|
| **29** | $N_3$ | | | 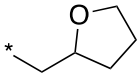 | 36.9 | 2.53 | 3.59 | 0.81 | 0.25 |
| **30** | $N_1$ | | | | 21.1 | 0.50 | | 1.08 | 0.27 |
| **31** | $N_3$ | | | 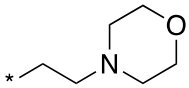 | 118.6 | 3.73 | 2.84 | 1.20 | 0.21 |
| **32** | $N_1$ | | | | 52.6 | 1.60 | | 1.46 | 0.23 |
| **33** | $N_3$ | | | 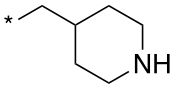 | 17.73 | 0.93 | 0.50 | 4.25 | 0.26 |
| **34** | $N_1$ | | | | 25.51 | 1.15 | | 4.09 | 0.25 |
| **35** | $N_3$ | | | 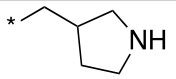 | 26.10 | 0.62 | - 0.28 | 4.86 | 0.27 |
| **36** | $N_1$ | | | | 45.65 | 1.78 | | 4.62 | 0.26 |
| **37** | $N_3$ | | | 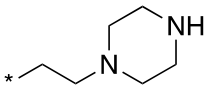 | 24.9 | 0.74 | 0.96 | 3.64 | 0.24 |
| **38** | $N_1$ | | | | 45.0 | 1.43 | | 3.39 | 0.23 |
| **37a** | $N_3$ | *F* | | | 5.2 | 0.23 | 0.97 | 4.32 | 0.28 |
| **39** | $N_3$ | | | 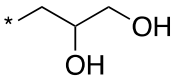 | 17.0 | 0.75 | 1.85 | 2.64 | 0.27 |
| **40** | $N_1$ | | | | 25.2 | 2.27 | | 2.35 | 0.25 |

[a] Reported $IC_{50}$ values are calculated from measurements performed in triplicates, in at least two separate experiments. 95 % confidence intervals of the values can be found in the Supporting Information. [b] $LogD_{7.4}$ were calculated using Chemicalize. [c] Residual activity of ~ 30 %. [d]NI: no inhibition. Unless indicated otherwise, Y and $R_2$ = H, X = CH.

**STD-NMR Study of Interaction Between the Active Site and the Inhibitor.** To better understand the observed SARs and notably how the nature and positioning of the lateral *N*-sidechain influenced the binding of the inhibitor inside the active pocket, we performed epitope mappings on several couples of regioisomers using saturation transfer difference NMR (STD-NMR). In STD-NMR, selective saturation of *h*TDO2 in solution is transferred to the bound ligand through intermolecular NOEs between protons of the inhibitor and the active site's residues. Consequently, the ligand's protons interacting more closely display intense STD signals, while a decrease in STD intensity correlates with lower interaction.[41] Due to solubility issues, we focused our investigation on compounds bearing solubilizing moieties to attain a high compound concentration (up to 200 $\mu$M) in aqueous buffer, suitable for the present evaluation. We mapped the epitopes of regioisomers **25 - 26**, **35 - 36** and **31 - 32** (**Figure 3**). Epitope mapping of all six compounds suggested that $N_3$-substitutions led to an improper position of the indole ring compared to $N_1$-substitutions (data regarding compounds **25 - 26** and **35 - 36** can be found in supporting information, **Figure S2**). Indeed, as pictured in **Figure 3**, epitope mapping on the different compounds showed that the indole ring displays the highest saturation transfer for protons $H_5$, $H_6$ and $H_7$ (around 100%). Concurrently, co-crystallographic structures of *h*TDO2 with L-Trp show that this part

of the indole tightly interacts with a cluster of several hydrophobic residues involving L120, F5, Y24, Y27 and L28.[39] In the case of L-Trp, the indole $H_2$ position is located very close to the heme.[39] Similarly, **26**, **36** and **32** all exhibited a saturation transfer of around 90 % for $H_2$. However, we observed that the less active $N_3$ substituted analogues **25**, **35** and **31**, systematically displayed a 20 to 30 % decrease in saturation transfer for $H_2$ compared to their regioisomers substituted in $N_1$. Overall, these results suggest a shift in the position of the indole core for $N_3$ substituted compounds, resulting in misplacement of $H_2$. This apparent shift of the indole position could, at least in part, explain the difference in activity between $N_1$ and $N_3$ substituted compounds.

Interestingly, the sidechain of the different isomers always showed a similar and low saturation transfer compared to the aromatic protons. Therefore, the nature of the sidechains does not appear to be useful for the interaction with *h*TDO2, which opens the door to further modulation to fine-tune this family of inhibitor physicochemical properties.

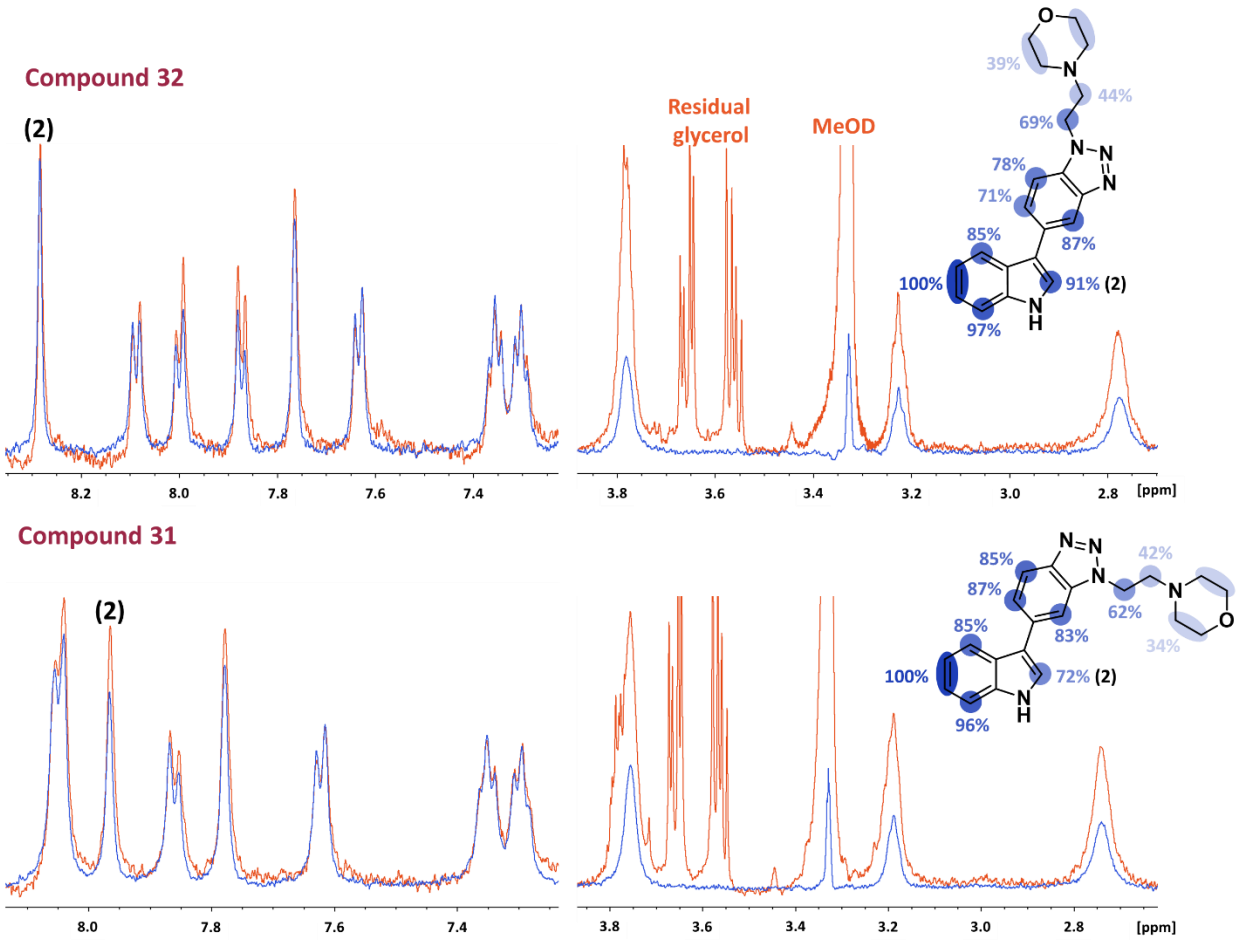

**Figure 3.** Epitope mapping for regioisomers **32** ($IC_{50}$ 52.6 µM (enz.), 1.6 µM (cell.) and **31** ($IC_{50}$ 118.6 µM (enz.), 3.7 µM (cell.). One-dimensional NMR $^{1}H$ proton spectra (blue) overlaid with STD spectra (orange). Corresponding compounds are represented above each set of spectra. Blue circles represent the protons at the designated position(s), with percentages represent STD intensity of the respective proton(s). Two of the ethylene protons could not be seen as their shift coincide with the water signal.

**Molecular docking**. Our molecular docking studies suggested two main hindrances for the accommodation of different ligands in the active site of *h*TDO2. The first identified hinder was Arg144, as a shift in its sidechain was required for the binding of the inhibitors. Displacement of this sidechain increased with the size of the *N*-substituent and was more important for $N_3$ regioisomers. We noticed that wider Arg144 shifts correlated with lower enzymatic activity. The second hinder was the flexible 338 – 346 loop, suggesting that an induced-fit type binding was perhaps needed for larger compounds. It was previously described that disordering of this loop allows NFK to diffuse out and enables de binding of a new L-Trp molecule.[39] Its mobility was particularly noticeable when *h*TDO2 was co-crystallized with an NLG919-type analog, widely opening the active site.[28]

Regioisomers displayed a similar binding pose, as shown in **Figure 4** for analogues **17** ($IC_{50}$(enz): 15.0 $\mu$M/ $IC_{50}$(cell): 0.44 $\mu$M) and **18** ($IC_{50}$(enz): 1.9 $\mu$M, $IC_{50}$(cell): 0.19 $\mu$M) with a particularly noticeable affinity difference. However, docking of $N_1$-substituted compounds resulted in a more favorable geometry for the indole core placement. Indeed, $N_3$-substituted compounds display a shift of the indole core from the position naturally adopted by the indole of L-Trp, with a shift of C2, disturbing the interaction with the aromatic hotspots. Regarding compounds bearing a longer sidechain with an H-bond donor (compounds **33** to **40**), our docking results suggested a possible interaction with the propionate of the heme or with an H-acceptor sidechain (such as Ser345) from the mobile loop. This interaction could potentially explain the slightly better activity observed for $N_3$ analogues.

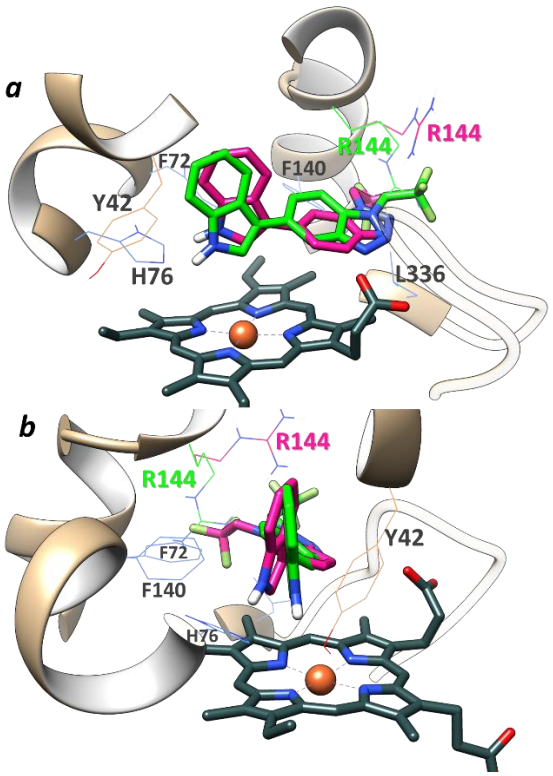


**Figure 4.** Molecular modeling of regioisomers **17** (pink) and **18** (green), bearing a trifluoroethyl from the front (***a***) and the side (***b***). (PDB code: 5TI9)[39]

**Phase I metabolic stability and electrophilic reactivity.** The potential reactivity of **LM10** as Michael acceptor was assessed with a thiol-trapping assay using cysteamine as S-nucleophile and compared to that of the unsubstituted benzotriazole **6**.[42–44] Following incubation with cysteamine, the $^{1}$H NMR spectrum of **LM10** quickly changed to reveal the apparition of several new aromatic signals. In contrast, the compound **6** spectrum stayed the same (**Figure 5**). Accordingly, LC/MS analysis of **LM10** ($[M + H]^{+}$= 230.1) confirmed the apparition of a secondary product ($[M + H]^{+}$= 305.1) upon cysteamine addition while **6** was not impacted.

Then, we evaluated the microsomal half-life of **LM10** and several representative benzotriazoles (**Table 3**). The recovery percentage of **LM10** after 24 hours remained close to the initial concentration. Regarding the present series, we noticed that the nature of the *N*-substituent was determinant for the recovery rate of the compounds. The presence of fluorine on the indole did not impact the microsomal

stability in compounds **8a** and **37a** compared to their non-fluorinated analogues. Furthermore, in isomers **37** and **38**, the localization of the *N*-substituent did not impact the microsomal stability.

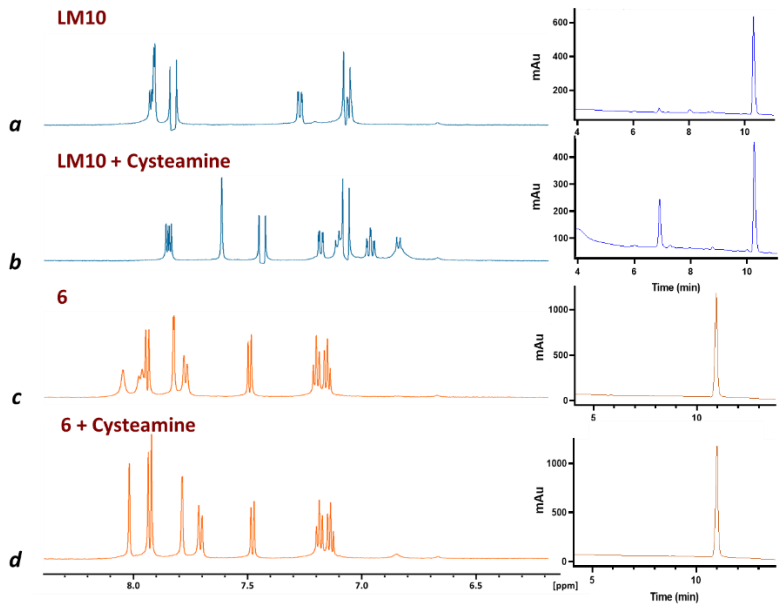


**Figure 5.** Aromatic regions of $^{1}$H NMR in DMSO-*d6* spectra of 1 mM of **LM10** (***a***) and **6** (***c***) before and after (***b, d***) addition of 10 equivalents of cysteamine. Spectra were recorded 30 minutes after the addition of cysteamine. Spectrum ***b*** (LM10 + cysteamine) shows several new aromatic signals, while proton integrations of compound **6** remain unchanged but displayed a slight shift in the presence of cysteamine.

**Table 3. Microsomal stabilities (half-lives) of representative compounds**

| N° | $N_x$ | $R_1$ | **Microsomal half-life**(min.) |
|---|---|---|---|
| **LM10** | / | / | > 1440 |
| **6** | / | H | 62 |
| **8** | $N_3$ | *$CH_3$ | 24 |
| **8a** | $N_3$ | *$CH_3$ | 22 |
| **18** | $N_1$ | *$CF_3$ | 45 |
| **26** | $N_1$ | * N | 43 |

| | | | |
|---|---|---|---|
| **35** | $N_3$ | 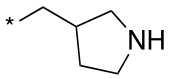 | > 1440 |
| **37** | $N_3$ | | > 1440 |
| **37a** | $N_3$ | 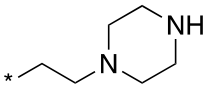 | > 1440 |
| **38** | $N_1$ | | > 1440 |

The stability values were obtained in duplicates in two separate experiments. Graphs of stability curves can be found in supporting information **(Figure S3).**

Overall, these data demonstrate that the structural rigidification results in a scaffold that does not exhibit Michael acceptor behavior. Nonetheless, the microsomal stability studies contrast our initial idea that this template rigidification would necessarily lead to more metabolically stable compounds. Indeed, the present series display considerable heterogeneity in metabolic stability, which appears heavily dependant on the nature of the *N*-substituent.

**Chemistry.** The target compounds were synthesized by Suzuki-Miyaura cross-coupling between halogenated benzotriazole analogs and the appropriate indole boronic ester.

Compounds **1 – 5** were obtained following the reaction between brominated isoquinolines or quinazolines and **41**. The synthesis of **680C91**-type analogues was performed using the same strategy, starting from **3** in the cross-coupling reactions (**Scheme 1**).

Several routes were attempted to synthesize compound **6**, bearing an unsubstituted benzotriazole, leading to the synthetic pathway depicted in **Scheme 2**. We used *p*-methoxybenzyl (PMB) as a protecting group for 5-Bromo-benzotriazole, which led to the formation of two regioisomers. Then, we performed the cross-coupling using the MIDA boronate **43** following a procedure adapted from *D.M. Knapp et al*.[45] The MIDA boronate allows a continuous release of the boronic acid over several hours. This unique capacity enabled us to obtain the cross-coupled product with an almost quantitative yield. The cross-coupled product was first deprotected from its phenylsulfonyl ($SO_2Ph$) using KOH, after what the PMB was removed in pure trifluoroacetic acid (TFA) at reflux temperature for 16 hours to

afford **6**. We noted that no degradation of the scaffold occurred despite the harsh basic and acidic conditions of both deprotection.

Two different routes, depicted in **Scheme 3** and **Scheme 4**, were used to synthesize *N*-substituted benzotriazoles, either by direct alkylation of commercially available 5-halo-benzotriazole (**Scheme 3**) or by nucleophilic aromatic substitution starting from bromofluoronitrobenzene derivatives (**Scheme 4**), followed by reduction of the aromatic nitro group and treatment of the resulting compounds by sodium nitrite in acetic acid to get the final alkylated benzotriazoles (**7b – 23b**, **17d – 40d**). To assess the substitution influence on the 6-membered ring, we took advantage of a highly electron-rich position between the halogen and the carbon between the two cycles to perform nitration using $KNO_3$ in $H_2SO_4$. A reduction using $Fe_{(s)}/NH_4Cl$ was then performed to reduce the aromatic nitro group (**Scheme 5**).

The halogenated benzotriazoles (**7b – 23b**, **17d – 40d**) were reacted with indole derivatives bearing a pinacol or MIDA boronate in the 3-position and a $SO_2Ph$ or a *tert*-butyloxycarbonyl (Boc) as a protecting group to afford the cross-coupled intermediates (**Scheme 6**). Finally, the target compounds **7 - 40** were eventually obtained after appropriate deprotection.

**Scheme 1. General synthetic procedure for compounds 1 - 5.**[a]

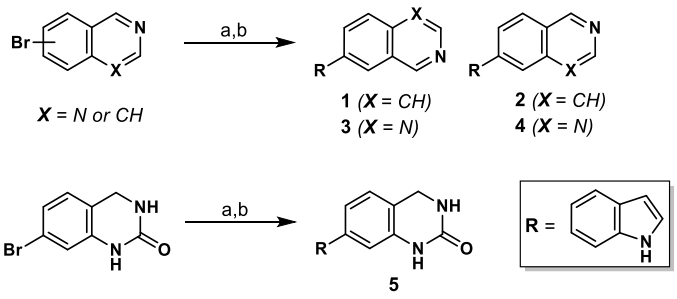


[a] Reagents and conditions: (a) **3** (1-(phenylsulfonyl)-3-(4,4,5,5-tetramethyl-1,3,2-dioxaborola*N*-2-yl)-1H-indole **42** (1.2 eq), 5 mol % $Pd(dppf)Cl_2$, 10 mol % SPhos, $K_3PO_4$ (2.0 eq), Dioxane/$H_2O$ (5:1), 60°C, 3-6h, Under $N_2$. (b) KOH 2.5M in MeOH/$H_2O$ (1:1), reflux 30 min. – 48h.

**Scheme 2. Synthesis of compound 5-(1H-indol-3-yl)-1H-benzotriazole (6).**[a]

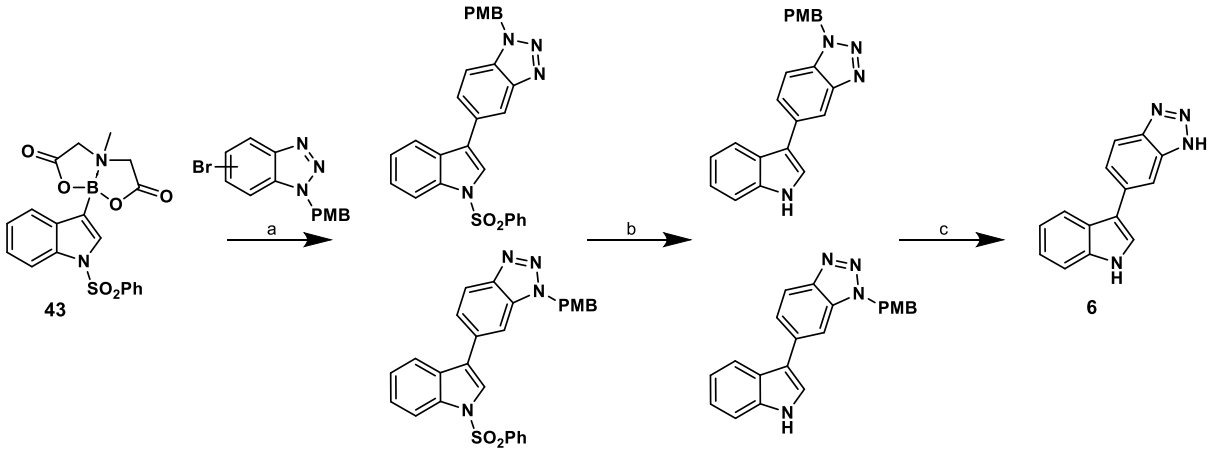


[a] Reagents and conditions: (a) 5 mol % $Pd(dppf)Cl_2$, 10 mol % SPhos, $K_3PO_4$ (2.0 eq), Dioxane/$H_2O$ (5:1), 60°C, 6h, Under $N_2$. (b) KOH 2.5M in $H_2O$/MeOH (1:1), reflux, 1h. (c) 100 % TFA, reflux, 16h.

**Scheme 3. Synthetic Routes for the *N*-substituted 5- and 6-halobenzotriazoles (7b – 9b, 13b – 15b, 21b – 22b).[a]**

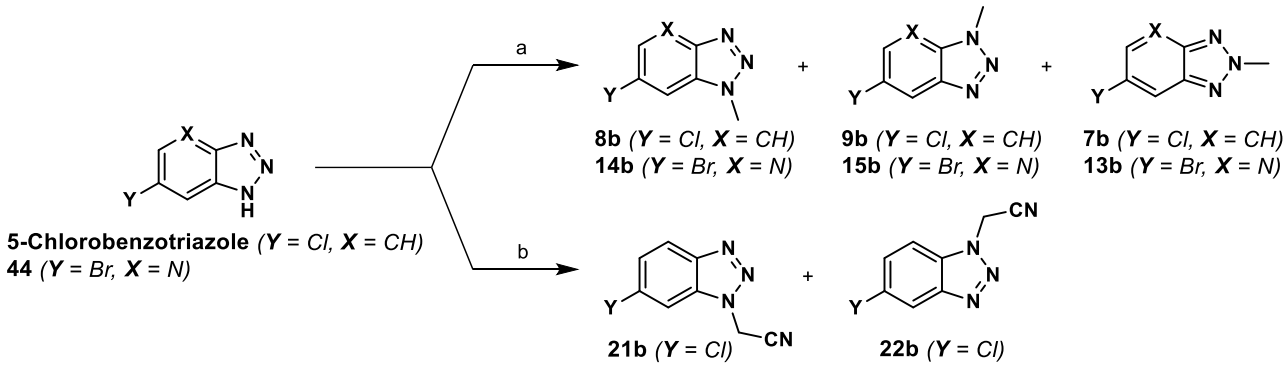


[a] Reagents and conditions: (a) $Me_2SO_4$ (1.6 eq), $NaOH_{aq}$ 2M, r.t., 1h30 (b) $ClCH_2CN$ (1.5 eq), $Et_3N$, DMF, reflux, 16h.

**Scheme 4. Synthetic Route for *N*-substituted 5-bromobenzotriazoles and 6-bromobenzotriazoles (17d – 40d).[a]**

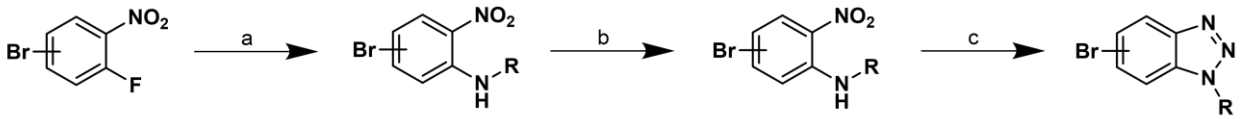


| R: | 6-Br | 5-Br | 6-Br | 5-Br | 6-Br | 5-Br |
|---|---|---|---|---|---|---|
| *2,2,2,-trifluoroethyl* | **17b** | **18b** | **17c** | **18c** | **17d** | **18d** |
| *cyclopropylmethyl* | **19b** | **20b** | **19c** | **20c** | **19d** | **20d** |
| *2-(dimethylamino)ethyl* | **25b** | **26b** | **25c** | **26c** | **25d** | **26d** |
| *(tetrahydrofuran-2-yl)methyl* | **27b** | **28b** | **27c** | **28c** | **27d** | **28d** |
| *(tetrahydrofuran-3-yl)methyl* | **29b** | **30b** | **29c** | **30c** | **29d** | **30d** |
| *2-morpholinoethyl* | **31b** | **32b** | **31c** | **32c** | **31d** | **32d** |
| *tert-butyl 4-ethylpiperidine-1-carboxylate* | **33b** | **34b** | **33c** | **34c** | **33d** | **34d** |
| *tert-butyl 3-ethylpyrrolidine-1-carboxylate* | **35b** | **36b** | **35c** | **36c** | **35d** | **36d** |
| *tert-butyl 4-ethylpiperazine-1-carboxylate* | **37b** | **38b** | **37c** | **38c** | **37d** | **38d** |
| *butane-1,2-diol* | **39b** | **40b** | **39c** | **40c** | **39d** | **40d** |

[a] Reagents and conditions: (a) primary amine derivative, $Et_3N$ (1.3 eq), EtOH or THF, r.t. or reflux, 30 min. – overnight; (b) $Fe_{(s)}$ (10 eq), EtOH/$H_2O$ (4:1), reflux, 30 min. – overnight; (c) $NaNO_2$ (2.5 eq), glacial acetic acid, sonication, r.t., 1h.

**Scheme 5. Synthetic Route for nitration and reduction to anilines of chloro-methyl-benzotriazoles.[a]**

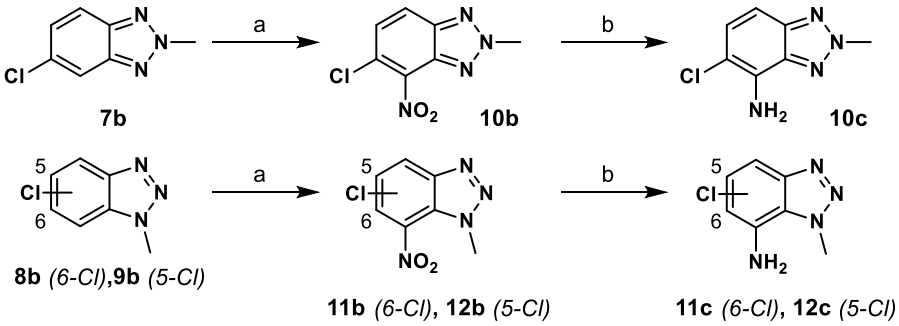


[a] Reagents and conditions: (a) $KNO_3$ (3.0 eq) in $H_2SO_4$, 50°C, 1h30 (b) $Fe_{(s)}$ (10.0 eq), EtOH/$H_2O$ (4:1), reflux, 30 min.

**Scheme 6. General synthetic procedure for cross-coupling and deprotection of 6-(1H-indol-3-yl)-benzotriazole derivatives.[a]**

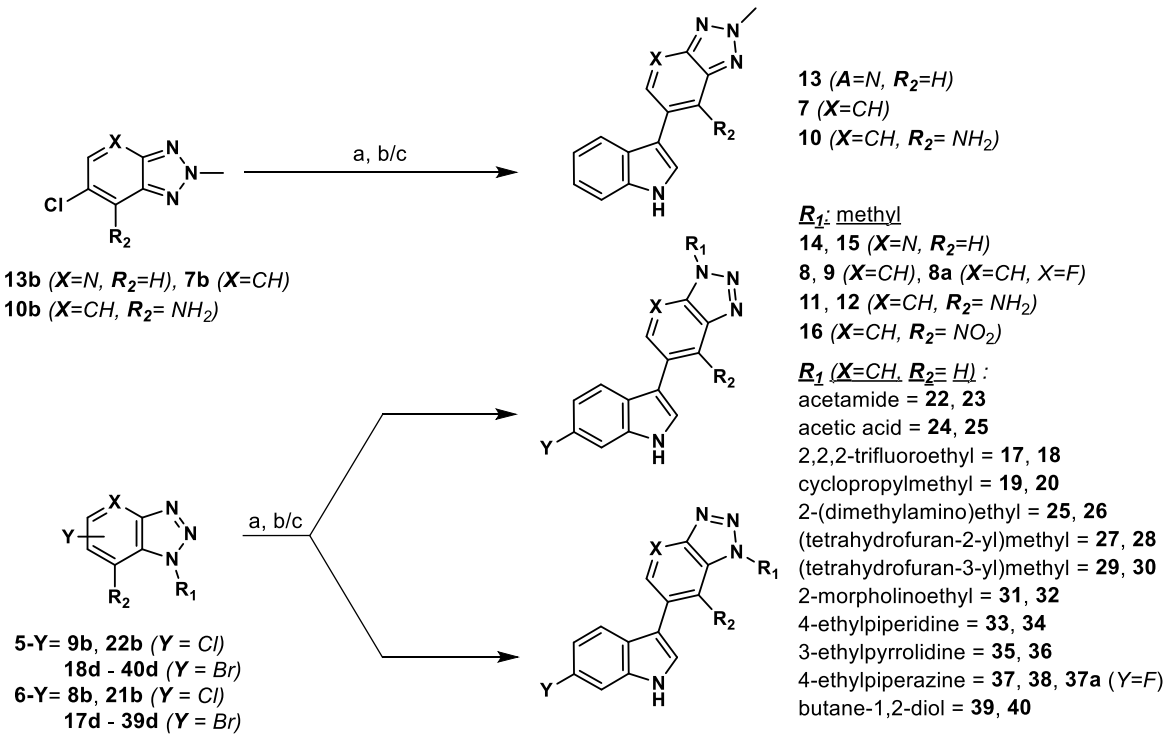


[a] Reagents and conditions: (a) Boronic ester derivative (**41**, **42** or **43)** (1.2 – 1.5 eq.), 5 mol % $Pd(dppf)Cl_2$, 10 mol % SPhos, $K_3PO_4$ (2.0 eq), Dioxane/$H_2O$ (5:1), 60°C, 3-6h, Under $N_2$. (b) HCl 4.0 M in MeOH/$H_2O$ (1:1), reflux, 30 min. – 5h for Boc deprotection, (c) KOH 2.5M in in MeOH/$H_2O$ (1:1) or 1 M TBAF in THF, reflux 30 min. – 48h. for $SO_2Ph$ deprotection.

## ■ CONCLUSIONS

In this work, we designed a series of original TDO2 inhibitors, devoid of the potentially problematic vinyl linker of the reference compound **LM10**. We evaluated these compounds through a SAR study completed by STD epitope mapping and stability evaluation. These compounds present a wide range of lipophilicity and various chemical characteristics, showing the possibility of fine-tuning these inhibitors' molecular and pharmacokinetic characteristics for potential ADME purposes. Compared to existing potent TDO2 inhibitors (**Figure 6a**), the present series shows similar or slightly better (**8a**) cellular affinities, up to the nanomolar range (**Figure 6b**). Previously, we reported that the enzyme seemed to be susceptible to small modifications of the inhibitor. However, we bring nuance to that affirmation, as TDO2 appears to allow bulkier substitutions for this series of compounds.

Interestingly, this series of compounds showed a systematically better activity on cells than on isolated enzyme. Such difference was previously observed for other indole-based patented TDO2 inhibitors.[33,46]

Moreover, other previous works preferred focusing on cellular activities and did not include enzymatic inhibition values (i.e., preclinical compound **PF06845102/EOS200809**, evaluated here in the biochemical assay, **Figure 6**).[25,27,28] Different parameters could account for this discrepancy. Firstly, the enzymatic assay that uses ascorbate, methylene blue, and catalase to maintain a reduced state could mimic poorly the physiological protein environment.[47] Furthermore, some inhibitors could also bind to the apo form of the protein, inhibiting its activity in a way the enzymatic assay would not detect.

Finally, the isoquinolines and quinazolines derivatives reported in this work (**1** – **5**) also constitute attractive, and highly functionalizable scaffolds for the future development of TDO2 inhibitors.

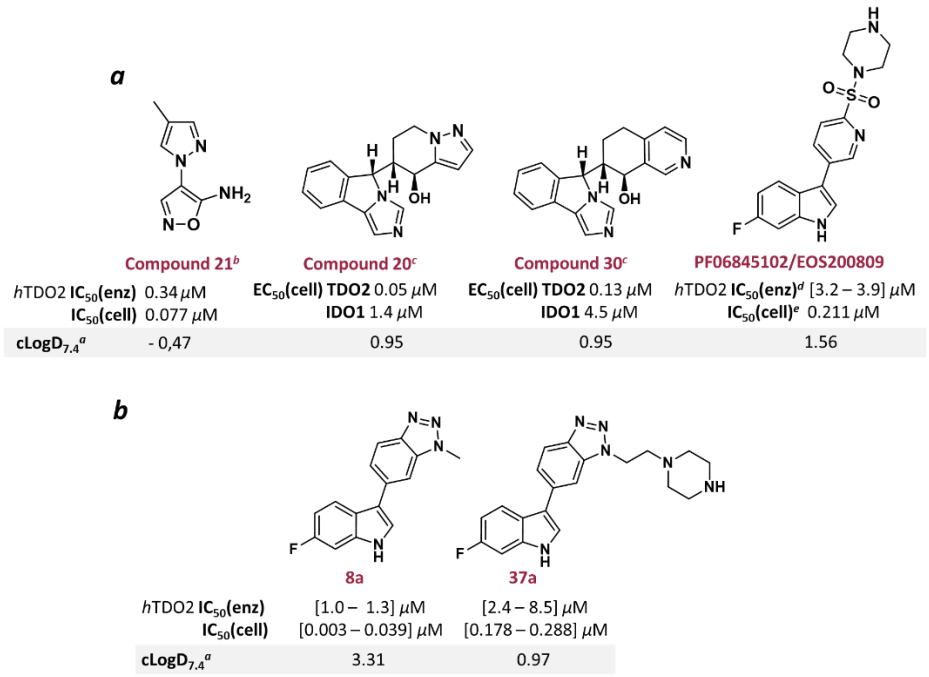


**Figure 6.** Examples of potent TDO2 inhibitors (**a**) and representative examples of the series developed in the present work (**8a** and **37a**). [a]$LogD_{7.4}$ were calculated using Chemicalize.[b] Compound **21** and its inhibition values are from Pei et al. 2018.[48] [c]Compounds **20**, **30** and their inhibition values are from Parr et al.[28] [d]Cellular potency of **PF06845102/EOS200809** is from Schramme et al. 2020.[25] [e]The biochemical $IC_{50}$ was measured in the present work.

## ■ EXPERIMENTAL SECTION

**Chemistry.** The following section comprise the general synthetic procedures used for the synthesis of compounds reported in this manuscript. Unless stated otherwise, reactions were performed under atmospheric pressure. Detailed experimental information and spectroscopic data of synthesized

compounds are supplied in the ***Supporting Information file***. LC-MS analysis was performed on an Agilent (1100 series) HPLC single quadrupole (InfinityLab, ESI+) system equipped with a Kinetex 5 µm EVO C18 (150 mm × 4,6 mm) using a gradient of distilled water + 0.1% TFA (buffer A) and acetonitrile + 0.1% TFA (buffer B). HPLC conditions for purity analysis were 5% B + 95% A at a flow rate of 1 mL/min, followed by an increase of solution B to 80% in 15 min (5%/min). The wavelength for UV detection was 254 nm and 210 nm. HPLC purities of final compounds that underwent biological assessment were ≥ 95%.

**The *N*-substituted benzotriazoles (18d – 40d) were synthesized using the following three step general procedure. (A)** To a 0.5 M solution of 4-bromo-1-fluoro-2-nitrobenzene or 4-bromo-2-fluoro-1-nitrobenzene (1 eq) in ethanol was added the primary amine (1.5 eq) and triethylamine (2 eq). The resulting mixture was sturred under reflux until complete conversion (30 min. - 16h), before being evaporated in vacuo. The residue was extracted using EtOAc and water and the organic layer was dried with $Na_2SO_4$ and concentrated to afford the desired compound, used in the next step without further purification (unless stated otherwise). **(B)** The nitro group of *N*-substituted 4-bromo-2-nitroaniline or 5-bromo-2-nitroaniline (1 eq) obtained in step **A** was reduced into an amine using iron powder (10 eq) in a mixture of $NH_4Cl_{sat.}$/EtOH (1:4) stirred under reflux for 30 min. to 16h. Upon complete conversion, the reaction mixture was filtrated over a celite pad, washed with EtOAc. After extraction, the organic layer was dried over $Na_2SO_4$ and concentrated in vacuo. Unless stated otherwise, the obtained residue was used for step **C** without further purification. **(C)** The cyclisation of mono *N*-substituted 4-bromobenzene-1, 2-diamine or 5-bromobenzene-1, 2-diamine was performed using $NaNO_2$ in acetic acid using a sonication bath for 30 min. - 1h. The reaction mixture was then poured onto ice water and extracted with EtOAc. The combined organic layers were washed with saturated $Na_2CO_3$ solution and Brine, dried with $Na_2SO_4$ and concentrated in vacuo. The *N*-substituted benzotriazole was purified using flash chromatography on silica gel with an EtOAc/cyclohexane gradient.

**General procedures nitration (D) of chloro-methyl-benzotriazoles. (D)** 2 mmol of the appropriate chloro-methyl-benzotriazole (**7b – 9b**) was dissolved in 3.5 mL of concentrated $H_2SO_4$. To this solution, 6.5 mmol of $KNO_3$ in concentrated $H_2SO_4$ were added dropwise. The resulting mixture was agitated for 1h30 at 50°C. After cooling down to room temperature, the reaction mixture was poured on ice, resulting in a precipitate formation (**10b – 12b**). The obtained powder was washed with water until neutrality. In accordance with the literature nitration of 5-chloro-2-methyl-2H-benzo[d][1,2,3]triazole (**7b**) led to the formation of a second di-nitrated product: 5-bromo-2-methyl-4,6-dinitro-2H-benzo[d][1,2,3]triazole in addition to the mono-nitrated 5-chloro-2-methyl-4-nitro-2H-benzo[d][1,2,3]triazole (**10b**).[49] The general reduction procedure **(C)** was used to reduce the nitrated chloro-methyl-benzotriazoles into *N*-methylbenzotriazol-4-amines (**10c – 12c**).

**General procedures for the Suzuki-Miyaura cross-coupling reaction.** Prior to the coupling procedures, the solvent 1,4-Dioxane and $K_3PO_4$ solution in water were degassed by atmosphere exchange with nitrogen in a sonication bath for 45 minutes. The cross-coupling procedure was adapted from DM Knapp et al.[45] We found that the use of Pd(dppf)$Cl_2$ as catalyst significantly increased the yield as compared to $Pd(OAc)_2$. **(E) Coupling procedure adapted for the use of a pinacol boronic ester (41, 42).** Aryl-halide (1mmol, 1 eq) and the boronic ester (1.6 eq), Pd(dppf)$Cl_2$ (5 mol %) and SPhos (10 mol %) were introduced into a 25 ml 2-neck round-bottom flask under inert atmosphere. Then, 10 mL of degassed dioxane were added and the reaction was left under agitation at r.t. for 10 minutes until dissolution of reactants. Finally, 2 mL of degassed distilled water containing $K_3PO_4$ (3.5 mmol) were added to the media and the reaction was stirred for 3 to 16h at 70°C. When the conversion was complete, the mixture was cooled to room temperature, diluted with 1N NaOH (10 mL) and extracted twice with 10 mL EtOAc. The combined organic fractions were dried over $Na_2SO_4$ and concentrated in vacuo. The obtained residue was purified by flash chromatography on silica gel with the appropriate gradient of EtOAc in cyclohexane to afford the cross-coupled protected intermediate. **(F) Coupling procedure adapted for the use of a MIDA boronate (43).** General procedure **(E)** was slightly adapted

when couplings were performed using MIDA boronate **43**. In this modified procedure **(F)** 1.2 eq of boronate and 7 eq of $K_3PO_4$ were used.

**General phenylsulfonyl ($SO_2Ph$) deprotection procedures of cross-coupled products.** Intermediates obtained using procedures **(F)** and **(E)**, bearing an $SO_2Ph$ protecting group were deprotected using deprotection procedures **(G)** or **(H)**, while Boc deprotection was performed using deprotection procedure **(I)**.

**Deprotection procedure G.** 0.5 mmol of starting compound were dissolved in 4 mL of a 1:1 solution of MeOH/$H_2O$ containing 2.5 M of KOH. The resulting mixture was refluxed until completion of the reaction (30 min. – 48h) to afford compounds **1** – **20**, **23** – **27**, **31** – **40**.

**Deprotection procedure H.** 0.5 mmol of starting compound were dissolved in 4 mL of a 1M solution of TBAF in THF. The resulting mixture was refluxed until completion of the reaction (2h. – 48h.) to afford compounds **21** – **22**, **28** – **30**.

**Deprotection procedure I.** 0.5 mmol of starting compound were dissolved in 4 mL of a 1:1 solution of MeOH/$H_2O$ containing 4 M of HCl. The resulting mixture was refluxed until completion of the reaction (30 min. – 48h.) to afford compounds **8a**, **37a**, **17** – **18**.

**Molecular Docking.** Molecular docking jobs were performed with AutodockVina 1.1.2,[50] using the disclosed tryptophan 2,3-dioxygenase structure (PDB ID: 5TI9)[39] with the orthosteric binding site occupied by natural ligand tryptophan, heme, and dioxygen. This structure was chosen as it displayed the full 338-346 loop that is part of this binding site. Hydrogens and charges were added then tryptophan and dioxygen were removed, centering the searching box 15 Å around this region. During the process, sidechain flexibility was allowed for several residues of the binding site and later on only for the Arg144 that appeared critical. Binding poses were analyzed for their binding mode and assessed in comparison with crystallized analog and with L-Trp.

**Protein Expression and Purification.** The sequence of the truncated form of *h*TDO2 in which 1–17 and 389–406 fragments were deleted (**His6Thrb-TDO2tr)**, [23] described by Batabyal and Yeh, was inserted in a pET-28 plasmid, ordered from Genecust. The recombinant plasmid was transferred into the *E. coli* strain BL21 (DE3) (Rosetta). The transformant was selected from a single colony on a LB kanamycin agar plate and was used to inoculate a LB medium (50 $\mu$g/mL kanamycin and 34 $\mu$g/mL chloramphenicol) and were cultured at 37 °C until an optical density of 0.6 was reached. The expression of *h*TDO2 was induced by isopropyl 1-thio β galacto-pyranoside (IPTG), with a final concentration of 1 mM. An aliquot of hemin in NaOH 0.5M, with a final concentration of 8–10 µM, was added to the culture. The culture was grown at 20 °C for 20 h. Cells were harvested by centrifugation at 5000 rpm, 4 °C for 25 min. Cell pellets were resuspended in a lysis buffer (Tris-HCl 50 mM, pH 8.5, $MgCl_2$ 10 mM, NaCl 300 mM, imidazole 5 mM, and glycerol 10%) supplemented with protease inhibitors (Roche) and then disrupted by sonication, followed by a centrifugation at 4 °C, 10 000 rpm for 30 min. The supernatant was collected and 1 $\mu$L/mL of supernatant of β-mercaptoethanol was added, before loading onto 1 mL of His-trap FF-crude columns (GE Healthcare) according to the manufacturer' 's instructions. Protein concentrations were measured using the Bradford method with the Biorad protein assay kit, and sample homogeneity was assessed using sulfate−polyacrylamide gel electrophoresis (SDS−PAGE) with Coomassie brilliant blue as a staining agent. Purified TDO2tr was then dialyzed overnight in a pH 7.6 buffer containing 50mM sodium phosphate, 100mM NaCl, 20% glycerol, and 10mM L-Trp. To ensure of the quality and proper folding of the purified enzyme, **Nano Differential Scanning Fluorimetry Experiments** were performed on a Tycho NT.6 device (NanoTemper Technologies). According to the standard manufacturer's procedures, samples were poured into capillaries and heated up to 95 °C in 3 min while following fluorescence emission at 330 and 350 nm. Melting temperatures were extracted from the derivative of the 350/330 nm fluorescence ratios upon increasing temperature.

**Nuclear Magnetic Resonance.** All experiments were performed at 277K on a Bruker Ascend Avance III 600 MHz system equipped with a broadband cryoprobe (Bruker). For 1D Saturation transfer difference

(STD) studies, samples were prepared at 200 $\mu$M in PBS with 5% deuterated methanol. The concentration of *h*TDO2$_{tr}$ was 15 µM. Ligand binding was detected using an STD stddiffesgp.3 sequence with a 2s saturation time. Water signal suppression was achieved using an excitatio*n*-sculpting scheme, and a 50 ms spinlock was used to suppress protein background signals. For each experiment, 2048 scans were collected for o*n*- and off-resonance experiments (respectively at 0 and 40 ppm) to achieve a sufficient signal to noise ratio for the epitope mapping.

**Enzymatic Assay.** All the graphs were obtained with GraphPadPrism 8 software (San Diego, CA). The UV spectra were recorded at room temperature on a Spectramax® M2E spectrophotometer (Molecular Devices, LLC, Sunnyvale, CA) in 96-well flat bottom plates. The assay was performed in a pH 6.5 potassium phosphate buffer (100 mM) at 37°C. The final concentrations in each well were: 100 $\mu$M of L-Trp, 20 mM of L-ascorbate, 10 $\mu$M of methylene blue, 150 nM of catalase, 3 % of DMSO containing the inhibitor and (optionally) 0.01 % v/v of Triton X-100. The assay was initiated by the adding 15 $\mu$L of buffer containing *h*TDO2$_{tr}$ (no L-Trp, no DMSO) to 85 $\mu$L of buffer (with L-Trp and the tested inhibitor concentration in DMSO). After 15 minutes, 20 $\mu$L 30 % m/v of trichloroacetic acid in water were added and the plates were heated at 65°C for 15 minutes. Then, 100 $\mu$L of a 2% m/v p-dimethylbenzaldehyde solution in pure acetic acid was added to each well. After 10 minutes, absorbance reading was performed at 490 nM.

**Cellular Assays.** The assay was performed in 96-well flat bottom plates seeded with $1 \times 10^5$ cells (P815B-hTDO, clone 19) in a final volume of 200 $\mu$L of Iscove's modified Dulbecco medium (GIBCO-Thermo Fisher Scientific; which contains 80 µM L-Trp) supplemented with 2% FCS in the presence of the TDO inhibitor at different concentrations (1–25,000 nM) for 7 hours when substrate consumption was below 25 %. Cells were centrifuged 10 min at 300 rcf, after what 60 $\mu$L of supernatant were collected and mixed with 60 $\mu$L of 12% (wt/vol) trichloroacetic acid. After centrifugation at 4°C, 23000 rcf, 70 $\mu$L of supernatant was diluted with 70 $\mu$L of Milli-Q $H_2O$. The resulting solution was used to quantify L-Trp and Kyn concentrations by ultra-performance liquid chromatography (UPLC) based on

the retention time and the UV absorption. Briefly, samples was injected into Kinetex 2.6 um EVO C18 100A (2,1 X 50) column (Phenomenex) and were eluted using a 1,7 min linear gradient of acetonitrile in water (5-50 %) containing 0.1 % trifluoroacetic acid at a flow-rate of 0,6 ml/min. The column eluent was monitored with UV detector at 280nm and 360 nm to detect L-Trp and Kyn, respectively.

For hIDO counter-screening (P815B-hIDO, clone 6), the same protocol was applied, but the plates were seeded with $2 \times 10^5$ cells and incubated for 24h in order to achieve a similar substrate consumption.

**In cellulo assessment of toxicity.** 100 $\mu$L (containing 80 $\mu$L of PBS, 20 $\mu$L of PMS and 1 $\mu$L of MTS) were added to wells containing $1x10^5$ cells in 100 $\mu$L in DMEM. After 2–4 h of incubation with MTS and PMS at 37 °C, absorbance at 490 nm was measured.

**Microsomal stability assay.** Liver microsomes (20 mg protein/ml), NADPH regenerating system solutions A & B and 10 mM stock compound solution (100% DMSO) are prepared. The reaction mixture finally contains 713 µL purified water, 200 µL 0.5 M potassium phosphate pH 7.4, 50 µL NADPH regenerating system solution A (BD Biosciences Cat. No. 451220), 10 µL NADPH regenerating system solution B (BD Biosciences Cat. No. 451200) and 2 µL of the compound stock solution (10 µM final concentration). A control experiment was realized for each compound by substituting NADPH regenerating solutions A and B for 60 µl of purified water. The reaction mixture is warmed to 37°C for 5 minutes in a water bath, and the reaction is initiated by the addition of 25 µL of liver microsomes (0.5 mg protein/ml final concentration). At different time points (0 min –60 min –180 min – 360 min – 24h), 100 µL is withdrawn and added to 400 µL cold acetonitrile on ice. Then the mixtures are centrifuged at 13 000 rpm for 5 min at 4°C. Finally, 450µl of the supernatant is recovered, evaporated using speedvac and evaluated by UPLC. 7-Ethoxycoumarine was used as a positive control.

## ■ AUTHOR INFORMATION

**Corresponding Author**

raphael.frederick@uclouvain.be

## ■ ACKNOWLEDGMENTS

This work was supported by the Belgian *Fonds National de la Recherche Scientifique* (F.R.S.-FNRS; Grants 3.05557.43, 28252254 and 32704190), the Belgian *Fondation contre le Cancer* (Large Equipment grant), the French Community of Belgium (ARC 14/19- 058), the *Fonds Spéciaux de recherche* (FSR) at UCLouvain, and a J. Maisin Foundation grant. Arina Kozlova and Léopold Thabault were PhD Fellows of the F.R.S.-FNRS. Léopold Thabault is currently a Postdoctoral Researcher of the Belgian *Fondation contre le Cancer*.

The authors thank Esra Yildiz, Bénédicte Tollet, Lionel Pochet and MSc students Kamie Peters and Lucie Jacques for their involvement in organic synthesis, technical assistance and fruitful discussions.

We acknowledge the Nuclear & Electron Spin Technologies Platform (NEST) platform for the access to the Bruker Ascend Avance III 600 MHz system equipped with a broadband cryoprobe (Bruker).

The Center for Protein Engineering (CIP) of University of Liège (ULg) is acknowledged for their expertise in hTDO2 production and purification.

## ■ ABBREVIATIONS USED

TDO2, Tryptophan 2,3-dioxygenase; L-Trp, L-Tryptophan; SMI, small-molecule inhibitor; ADME, absorption, distribution, metabolism and excretion; KP, tryptopha*n*-kynurenine pathway; IDO1, indoleamine-2,3-dioxygenase 1; KMO, kynurenine-3-monooxygenase ; KYN, kynurenine ; AhR, aryl hydrocarbon receptor ; GCN2, general control nonderepressible 2 ; $T_{reg}$, regulatory T-cells ; NK, natural killer cell ; MDSCs, myeloid-derived suppressor cells; LE, ligand efficiency ; LLE, lipophilic ligand efficiency; NMR, nuclear magnetic resonance; STD, saturation transfer difference; NOE, nuclear overhauser effect.

## ■ ASSOCIATED CONTENT

Detailed procedures and analysis of the synthesized compounds

Supporting figures and tables as well as HPLC traces for lead compounds

Coordinates information for structure representation (PDB)

Molecular formula strings of synthesized compounds (CSV)

## ■ REFERENCES

(1) Fares, C. M.; Van Allen, E. M.; Drake, C. G.; Allison, J. P.; Hu-Lieskovan, S. Mechanisms of Resistance to Immune Checkpoint Blockade: Why Does Checkpoint Inhibitor Immunotherapy Not Work for All Patients? *Am. Soc. Clin. Oncol. Educ. Book* **2019**, No. 39, 147–164.

(2) Klemen, N. D.; Wang, M.; Feingold, P. L.; Cooper, K.; Pavri, S. N.; Han, D.; Detterbeck, F. C.; Boffa, D. J.; Khan, S. A.; Olino, K.; Clune, J.; Ariyan, S.; Salem, R. R.; Weiss, S. A.; Kluger, H. M.; Sznol, M.; Cha, C. Patterns of Failure after Immunotherapy with Checkpoint Inhibitors Predict

Durable Progression-Free Survival after Local Therapy for Metastatic Melanoma. *Journal for Immunother. cancer* **2019**, *7* (1), 196.

(3) Kerr, W. G.; Chisholm, J. D. The Next Generation of Immunotherapy for Cancer: Small Molecules Could Make Big Waves. *J. Immunol.* **2019**, *202* (1), 11–19.

(4) van der Zanden, S. Y.; Luimstra, J. J.; Neefjes, J.; Borst, J.; Ovaa, H. Opportunities for Small Molecules in Cancer Immunotherapy. *Trends Immunol.* **2020**, *41* (6), 493–511.

(5) Cheng, B.; Yuan, W. E.; Su, J.; Liu, Y.; Chen, J. Recent Advances in Small Molecule Based Cancer Immunotherapy. *Eur. J. Med. Chem.* **2018**, *157*, 582–598.

(6) Platten, M.; Nollen, E. A. A.; Röhrig, U. F.; Fallarino, F.; Opitz, C. A. Tryptophan Metabolism as a Common Therapeutic Target in Cancer, Neurodegeneration and Beyond. *Nat. Rev. Drug Discov.* **2019**, *18* (5), 379–401.

(7) Opitz, C. A.; Somarribas Patterson, L. F.; Mohapatra, S. R.; Dewi, D. L.; Sadik, A.; Platten, M.; Trump, S. The Therapeutic Potential of Targeting Tryptophan Catabolism in Cancer. *Br. J. Cancer* **2020**, *122* (1), 30–44.

(8) Routy, J. P.; Routy, B.; Graziani, G. M.; Mehraj, V. The Kynurenine Pathway Is a Double-Edged Sword in Immune-Privileged Sites and in Cancer: Implications for Immunotherapy. *Int. J. Tryptophan Res.* **2016**, *9* (1), 67–77.

(9) Munn, D. H.; Shafizadeh, E.; Attwood, J. T.; Bondarev, I.; Pashine, A.; Mellor, A. L. Inhibition of T Cell Proliferation by Macrophage Tryptophan Catabolism. *J. Exp. Med.* **1999**, *189* (9), 1363–1372.

(10) Munn, D. H.; Sharma, M. D.; Baban, B.; Harding, H. P.; Zhang, Y.; Ron, D.; Mellor, A. L. GCN2 Kinase in T Cells Mediates Proliferative Arrest and Anergy Induction in Response to Indoleamine 2,3-Dioxygenase. *Immunity* **2005**, *22* (5), 633–642.

(11) Metz, R.; Rust, S.; DuHadaway, J. B.; Mautino, M. R.; Munn, D. H.; Vahanian, N. N.; Link, C. J.; Prendergast, G. C. IDO Inhibits a Tryptophan Sufficiency Signal That Stimulates MTOR: A Novel IDO Effector Pathway Targeted by D-1-Methyl-Tryptophan. *Oncoimmunology* **2012**, *1* (9), 1460–1468.

(12) Fallarino, F.; Grohmann, U.; You, S.; McGrath, B. C.; Cavener, D. R.; Vacca, C.; Orabona, C.; Bianchi, R.; Belladonna, M. L.; Volpi, C.; Santamaria, P.; Fioretti, M. C.; Puccetti, P. The Combined Effects of Tryptophan Starvation and Tryptophan Catabolites Down-Regulate T Cell Receptor ζ-Chain and Induce a Regulatory Phenotype in Naive T Cells. *J. Immunol.* **2006**, *176* (11), 6752–6761.

(13) Mezrich, J. D.; Fechner, J. H.; Zhang, X.; Johnson, B. P.; Burlingham, W. J.; Bradfield, C. A. An Interaction between Kynurenine and the Aryl Hydrocarbon Receptor Can Generate Regulatory T Cells. *J. Immunol.* **2010**, *185* (6), 3190–3198.

(14) Liu, Y.; Liang, X.; Dong, W.; Fang, Y.; Lv, J.; Zhang, T.; Fiskesund, R.; Xie, J.; Liu, J.; Yin, X.; Jin, X.; Chen, D.; Tang, K.; Ma, J.; Zhang, H.; Yu, J.; Yan, J.; Liang, H.; Mo, S.; Cheng, F.; Zhou, Y.; Zhang, H.; Wang, J.; Li, J.; Chen, Y.; Cui, B.; Hu, Z. W.; Cao, X.; Xiao-Feng Qin, F.; Huang, B. Tumor-Repopulating Cells Induce PD-1 Expression in CD8+ T Cells by Transferring Kynurenine and AhR Activation. *Cancer Cell* **2018**, *33* (3), 480–494.

(15) Muller, A. J.; Sharma, M. D.; Chandler, P. R.; DuHadaway, J. B.; Everhart, M. E.; Johnson, B. A.; Kahler, D. J.; Pihkala, J.; Soler, A. P.; Munn, D. H.; Prendergast, G. C.; Mellor, A. L. Chronic Inflammation That Facilitates Tumor Progression Creates Local Immune Suppression by Inducing Indoleamine 2,3 Dioxygenase. *Proc. Natl. Acad. Sci. U. S. A.* **2008**, *105* (44), 17073–17078.

(16) Prendergast, G. C.; Mondal, A.; Dey, S.; Laury-Kleintop, L. D.; Muller, A. J. Inflammatory Reprogramming with IDO1 Inhibitors: Turning Immunologically Unresponsive 'Cold' Tumors 'Hot.' *Trends Cancer.* **2018**, *4* (1), 38–58.

(17) Terness, P.; Bauer, T. M.; Röse, L.; Dufter, C.; Watzlik, A.; Simon, H.; Opelz, G. Inhibition of Allogeneic T Cell Proliferation by Indoleamine 2,3-Dioxygenase-Expressing Dendritic Cells: Mediation of Suppression by Tryptophan Metabolites. *J. Exp. Med.* **2002**, *196* (4), 447–457.

(18) Uyttenhove, C.; Pilotte, L.; Théate, I.; Stroobant, V.; Colau, D.; Parmentier, N.; Boon, T.; Van den Eynde, B. J. Evidence for a Tumoral Immune Resistance Mechanism Based on Tryptophan Degradation by Indoleamine 2,3-Dioxygenase. *Nat. Med.* **2003**, *9* (10), 1269–1274.

(19) Van Den Eynde, B. J.; Van Baren, N.; Baurain, J. F. Is There a Clinical Future for IDO1 Inhibitors after the Failure of Epacadostat in Melanoma? *Annu. Rev. Cancer Biol.* **2020**, *4*, 241–256.

(20) Röhrig, U. F.; Majjigapu, S. R.; Reynaud, A.; Pojer, F.; Dilek, N.; Reichenbach, P.; Ascencao, K.; Irving, M.; Coukos, G.; Vogel, P.; Michielin, O.; Zoete, V. Azole-Based Indoleamine 2,3-Dioxygenase 1 (IDO1) Inhibitors. *J. Med. Chem.* **2021**, *64* (4), 2205–2227.

(21) Klaessens, S.; Stroobant, V.; Hoffmann, D.; Gyrd-Hansen, M.; Pilotte, L.; Vigneron, N.; De Plaen, E.; Van den Eynde, B. J. Tryptophanemia Is Controlled by a Tryptophan-Sensing Mechanism Ubiquitinating Tryptophan 2,3-Dioxygenase. *Proc. Natl. Acad. Sci.* **2021**, *118* (23), e2022447118.

(22) Meng, B.; Wu, D.; Gu, J.; Ouyang, S.; Ding, W.; Liu, Z. J. Structural and Functional Analyses of Human Tryptophan 2,3-Dioxygenase. *Proteins.* **2014**, *82* (11), 3210–3216.

(23) Batabyal, D.; Yeh, S. R. Substrate-Protein Interaction in Human Tryptophan Dioxygenase: The Critical Role of H76. *J. Am. Chem. Soc.* **2009**, *131* (9), 3260–3270.

(24) Pilotte, L.; Larrieu, P.; Stroobant, V.; Colau, D.; Dolušić, E.; Frédérick, R.; De Plaen, E.; Uyttenhove, C.; Wouters, J.; Masereel, B.; Van Den Eynde, B. J. Reversal of Tumoral Immune Resistance by Inhibition of Tryptophan 2,3-Dioxygenase. *Proc. Natl. Acad. Sci. U. S. A.* **2012**, *109* (7), 2497–2502.

(25) Schramme, F.; Crosignani, S.; Frederix, K.; Hoffmann, D.; Pilotte, L.; Stroobant, V.; Preillon, J.;

Driessens, G.; van den Eynde, B. J. Inhibition of Tryptophan-Dioxygenase Activity Increases the Antitumor Efficacy of Immune Checkpoint Inhibitors. *Cancer Immunol. Res.* **2020**, *8* (1), 32–45.

(26) Hoffmann, D.; Dvorakova, T.; Stroobant, V.; Bouzin, C.; Daumerie, A.; Solvay, M.; Klaessens, S.; Letellier, M. C.; Renauld, J. C.; van Baren, N.; Lelotte, J.; Marbaix, E.; van den Eynde, B. J. Tryptophan 2,3-Dioxygenase Expression Identified in Human Hepatocellular Carcinoma Cells and in Intratumoral Pericytes of Most Cancers. *Cancer Immunol. Res.* **2020**, *8* (1), 19–31.

(27) Kozlova, A.; Frédérick, R. Current State on Tryptophan 2,3-Dioxygenase Inhibitors: A Patent Review. *Expert Opin. Ther. Pat.* **2019**, *29* (1), 11–23.

(28) Parr, B. T.; Pastor, R.; Sellers, B. D.; Pei, Z.; Jaipuri, F. A.; Castanedo, G. M.; Gazzard, L.; Kumar, S.; Li, X.; Liu, W.; Mendonca, R.; Pavana, R. K.; Potturi, H.; Shao, C.; Velvadapu, V.; Waldo, J. P.; Wu, G.; Yuen, P. W.; Zhang, Z.; Zhang, Y.; Harris, S. F.; Oh, A. J.; Dipasquale, A.; Dement, K.; La, H.; Goon, L.; Gustafson, A.; Vanderporten, E. C.; Mautino, M. R.; Liu, Y. Implementation of the CYP Index for the Design of Selective Tryptophan-2,3-Dioxygenase Inhibitors. *ACS Med. Chem. Lett.* **2020**, *11* (4), 541–549.

(29) Yang, D.; Zhang, S.; Fang, X.; Guo, L.; Hu, N.; Guo, Z.; Li, X.; Yang, S.; He, J. C.; Kuang, C.; Yang, Q. N-Benzyl/Aryl Substituted Tryptanthrin as Dual Inhibitors of Indoleamine 2,3-Dioxygenase and Tryptophan 2,3-Dioxygenase. *J. Med. Chem.* **2019**, *62* (20), 9161–9174.

(30) Li, Y.; Zhang, S.; Wang, R.; Cui, M.; Liu, W.; Yang, Q.; Kuang, C. Synthesis of Novel Tryptanthrin Derivatives as Dual Inhibitors of Indoleamine 2,3-Dioxygenase 1 and Tryptophan 2,3-Dioxygenase. *Bioorganic Med. Chem. Lett.* **2020**, *30* (11).

(31) Dolusic, E.; Larrieu, P.; Moineaux, L.; Stroobant, V.; Pilotte, L.; Colau, D.; Pochet, L.; Eynde, V. Den; Masereel, B.; Wouters, J.; Frédérick, R. 3- ( 2- ( Pyridyl ) Ethenyl ) Indoles as Potential Anticancer Immunomodulators. *J. Med. Chem.* **2011**, *54*, 5320–5334.

(32) Pham, K. N.; Lewis-Ballester, A.; Yeh, S. R. Conformational Plasticity in Human Heme-Based

Dioxygenases. *J. Am. Chem. Soc.* **2021**, *143* (4), 1836–1845.

(33) ITEOS Therapeutics. Novel 3-Indol Substituted Derivatives, Pharmaceutical Compositions and Methods for Use. WO2015140717 (2015).

(34) Takikawa, O.; Kuroiwa, T.; Yamazaki, F.; Kido, R. Mechanism of Interferon-γ Action. Characterization of Indoleamine 2,3-Dioxygenase in Cultured Human Cells Induced by Interferon -γ and Evaluation of the Enzyme-Mediated Tryptophan Degradation in Its Anticellular Activity. *J. Biol. Chem.* **1988**, *263* (4), 2041–2048.

(35) Röhrig, U. F.; Majjigapu, S. R.; Vogel, P.; Zoete, V.; Michielin, O. Challenges in the Discovery of Indoleamine 2,3-Dioxygenase 1 (IDO1) Inhibitors. *J. Med. Chem.* **2015**, *58* (24), 9421–9437.

(36) Schultes, S.; De Graaf, C.; Haaksma, E. E. J.; De Esch, I. J. P.; Leurs, R.; Krämer, O. Ligand Efficiency as a Guide in Fragment Hit Selection and Optimization. *Drug Discov. Today Technol.* **2010**, *7* (3), 157–162.

(37) Hopkins, A. L.; Keserü, G. M.; Leeson, P. D.; Rees, D. C.; Reynolds, C. H. The Role of Ligand Efficiency Metrics in Drug Discovery. *Nat. Rev. Drug Discov.* **2014**, *13* (2), 105–121.

(38) Johnson, T. W.; Gallego, R. A.; Edwards, M. P. Lipophilic Efficiency as an Important Metric in Drug Design. *J. Med. Chem.* **2018**, *61* (15), 6401–6420.

(39) Lewis-Ballester, A.; Forouhar, F.; Kim, S. M.; Lew, S.; Wang, Y.; Karkashon, S.; Seetharaman, J.; Batabyal, D.; Chiang, B. Y.; Hussain, M.; Correia, M. A.; Yeh, S. R.; Tong, L. Molecular Basis for Catalysis and Substrate-Mediated Cellular Stabilization of Human Tryptophan 2,3-Dioxygenase. *Sci. Rep.* **2016**, *6*, 1–13.

(40) Dolušić, E.; Larrieu, P.; Moineaux, L.; Stroobant, V.; Pilotte, L.; Colau, D.; Pochet, L.; Van Den Eynde, B.; Masereel, B.; Wouters, J.; Frédérick, R. Tryptophan 2,3-Dioxygenase (TDO) Inhibitors. 3-(2-(Pyridyl)Ethenyl)Indoles as Potential Anticancer Immunomodulators. *J. Med. Chem.* **2011**, *54* (15), 5320–5334.

(41) Mayer, M.; Meyer, B. Group Epitope Mapping by Saturation Transfer Difference NMR to Identify Segments of a Ligand in Direct Contact with a Protein Receptor. *J. Am. Chem. Soc.* **2001**, *123* (25), 6108–6117.

(42) Avonto, C.; Taglialatela-Scafati, O.; Pollastro, F.; Minassi, A.; Di-Marzo, V.; De-Petrocellis, L.; Appendino, G. An NMR Spectroscopic Method to Identify and Classify Thiol-Trapping Agents: Revival of Michael Acceptors for Drug Discovery? *Angew. Chemie - Int. Ed.* **2011**, *50* (2), 467–471.

(43) Al-Rifai, N.; Rücker, H.; Amslinger, S. Opening or Closing the Lock? When Reactivity Is the Key to Biological Activity. *Chem. Eur. J.* **2013**, *19* (45), 15384–15395.

(44) Jackson, P. A.; Widen, J. C.; Harki, D. A.; Brummond, K. M. Covalent Modifiers: A Chemical Perspective on the Reactivity of α,β-Unsaturated Carbonyls with Thiols via Hetero-Michael Addition Reactions. *J. Med. Chem.* **2017**, *60* (3), 839–885.

(45) Knapp, D. M.; Gillis, E. P.; Burke, M. D. A General Solution for Unstable Boronic Acids: Slow-Release Cross-Coupling from Air-Stable MIDA Boronates. *J. Am. Chem. Soc.* **2009**, *131* (20), 6961–6963.

(46) ITEOS Therapeutics. Novel 3-(Indol-3-yl)-Pyridine Derivatives, Pharmaceutical Compositions and Methods for Use. US2015225367 (2015).

(47) Röhrig, U. F.; Majjigapu, S. R.; Vogel, P.; Zoete, V.; Michielin, O. Challenges in the Discovery of Indoleamine 2,3-Dioxygenase 1 (IDO1) Inhibitors. *J. Med. Chem.* **2015**, *58* (24), 9421–9437.

(48) Pei, Z.; Mendonca, R.; Gazzard, L.; Pastor, R.; Goon, L.; Gustafson, A.; Vanderporten, E.; Hatzivassiliou, G.; Dement, K.; Cass, R.; Yuen, P. W.; Zhang, Y.; Wu, G.; Lin, X.; Liu, Y.; Sellers, B. D. Aminoisoxazoles as Potent Inhibitors of Tryptophan 2,3-Dioxygenase 2 (TDO2). *ACS Med. Chem. Lett.* **2018**, *9* (5), 417–421.

(49) Carta, A.; Piras, S.; Boatto, G.; Paglietti, G. 1H,6H-Triazolo[4,5-e]Benzotriazole-3-Oxides and

5,5’-(Z)-Diazene-1,2-Diylbis(2-Methyl-2H-1,2,3-Benzotriazole) Derived from Chloronitrobenzotriazoles and Hydrazine. *Heterocycles* **2005**, *65* (10), 2471–2481.

(50) Trott, O.; Olson, A. J. AutoDock Vina: Improving the Speed and Accuracy of Docking with a New Scoring Function, Efficient Optimization, and Multithreading. *J. Comput. Chem.* **2009**, *31* (2), 455–461.